PCCP

Effect of Iron Doping on Protein Molecular Conductance

Journal:	*Physical Chemistry Chemical Physics*
Manuscript ID	CP-ART-01-2018-000656.R2
Article Type:	Paper
Date Submitted by the Author:	16-Apr-2018
Complete List of Authors:	Lebedev, Nikolai; NRL, Griva, Igor; George Mason University Blom, Anders; Quantumwise AS Tender, Leonard; Naval Research Laboratory, Center for Bio/Molecular Science + Engineering

PCCP

ARTICLE

Effect of Iron Doping on Protein Molecular Conductance

Nikolai Lebedev,*[a] Igor Griva,[b] Anders Blom,[c] and Leonard M. Tender[a]

Received 00th January 20xx,
Accepted 00th January 20xx

DOI: 10.1039/x0xx00000x

www.rsc.org/

Protein molecular conductance attracts researcher's attention for the possibility of the construction of innovative flexible biocompatible nanoscale electronic devices and smart hybrid materials. Due to protein complexity, most evaluations of protein conductivity are based on simple estimation of protein molecular orbital energy levels and spatial distribution without analysing protein interaction with electrodes and calculation of the rates of electron transfer (ET). In the present work, we include in our density functional theory (DFT) analysis an approach based on non-equilibrium Green's function (NEGF) allowing for calculation from the first principles the molecule interaction with electrodes and thus the role of electrode materials, Fermi level, thermal distribution of electronic energy levels, and the coupling efficiency between the molecule and the electrodes. Compared to proteins studied so far, mainly artificial peptides, heme-containing cytochromes, and bacterial pili, we choose for our calculation rubredoxin. Rubredoxin contains a non-heme iron that, as we have discovered recently, can be involved in extracellular ET in electroactive bacterial biofilms (Yates et. al. 2016). Our calculations show that an iron atom incorporated into the protein structure as an iron-sulfur cluster opens a transmission path at the energy corresponding to the Fermi level of the electrodes. This allows the protein to become an extremely efficient conductor at very low bias voltages (<±350 mV). Calculation of the role of protein amino acids based on the local density of states and electron transfer paths reveals that neither aromatic amino acid Tyr nor Phe at any ring orientation participate in coherent ET through the FeS cluster of the protein. Moreover, direct ET through surrounding amino acids, bypassing FeS, is possible only at biases ±1.5 to ±2 V. Polar amino acid Asn might participate in ET at these bias voltages. The conductivity of the protein core substantially depends on the polarity of the applied electric field, allowing for unidirectional ET and operation of the protein as a molecular rectifier. These results can be used for wise *de novo* design of proteins for molecular electronics and cellular energy converting devices, particularly for utilization of iron doping in the construction of conductive protein wires.

INTRODUCTION

Protein electronics is a new branch of molecular electronics which goal is to analyze the electron transport mechanisms and utilize the gained knowledge for the construction of robust super small flexible electronic materials and bioinorganic hybrids, including

[a] Center for Bio-Molecular Science and Engineering, U.S. Naval Research Laboratory, Washington, DC, 20375.
[b] Department of Mathematical Sciences and Center of Simulation and Modeling, George Mason University, Fairfax, Virginia, 22030.
[c] QuantumWise, Fruebjergvej 3, Copenhagen, DK-2100, Denmark.

† Footnotes relating to the title and/or authors should appear here.
Electronic Supplementary Information (ESI) available: Projected DOS of charged Asn and aromatic amino acids Phe and Tyt; Projected DOS of s, p and d orbitals of FeS cluster; The effect of temperature (300K vs 100K) on Rd ETS; Estimation of the number of channels contributing to the main transmission bands; Spatial distribution of molecular transmission eigenstate at +0.032 eV. See DOI: 10.1039/x0xx00000x

sensors, actuators, electrochemical cell, or catalytic devices. A lot of insight has been gained from experimentally observed electron transfer (ET) through proteins, including the discovery of super-fast (femtosecond) photoinduced electron transfer within photosynthetic proteins [1] and super long (up to hundred microns) ET in bacterial biofilms. [2-4] A theoretical interpretation of the mechanisms of ET within and between proteins in solution has been developed, especially in the framework of Marcus formalism, treating ET in individual proteins and their complexes as a set of coupled redox centers. [5-14] In the framework of Landauer formalism describing ET between proteins and solid state electrodes as a coherent tunneling process [15-18] the interpretation of protein conductance faces problems coming from the fact that biological molecules are not simple periodic structures, like metals, semiconductors, or carbon materials, but heteroatomic highly spatially irregular systems. [18-20] This analysis is also complicated by the fact that the principles of operation of inorganic and soft biological materials differ substantially [21-24] that makes problematic describing efficient energy and information transfer between them as a simple electrical contact.

Recently, we applied the Landauer formalism for a detailed analysis of ET through a protein placed between two inorganic electrodes. Our approach is based on density functional theory (DFT), includes non-equilibrium Green's function (NEGF) and takes into account spatially resolved protein and electrode energy levels, molecular orbital (MO) delocalization through protein amino acids affecting the distance needed for electron tunneling between them, the role of the tunneling barrier height (transfer through space vs. through the protein backbone) and the role of specific amino acids in the formation of electrostatic traps and loops in the ET paths. [25] Using *Geobacter sulfurreducens* pilA protein as a model system, we demonstrated that the long-range ET through the protein that does not have iron cannot occur by coherent tunneling, but requires taking into account sequential electron hopping and demands relatively high bias voltages. [25] Our results showed that protein parts which do not have iron mainly act as insulators at low biases due to the high LUMO-HOMO energy gap, insufficient MO delocalization needed for substantial reduction of the tunnelling through space, and inefficient coupling between the protein and the electrodes. In addition, positively charged amino acids in the protein act as energy traps which prevent coherent electron transfer at low bias voltages. [25] When we analyzed ET through heme (an iron-chelating porphyrin) connected to carbon nanotube (CNT) electrodes by two amino acids (His), we showed that ET through the porphyrin in this configuration is highly efficient at low biases. We showed that the efficiency of ET through iron atom substantially depends on the heme orientation relative to the direction of ET and is maximal at heme oriented orthogonally to the current direction. [26] In this orientation, the ET through a single iron atom can be controlled by the surrounding tetrapyrrole ring, allowing for the device operation as a single atomic field effect transistor. [26]

To understand the mechanism of iron-induced conductivity of proteins, in the present work we analyze the role of an iron-sulfur cluster in ET through a non-heme Fe protein, rubredoxin. [27, 28] This protein is the smallest iron-sulfur protein which has diverse biological functions, from mediation of ET in energetic metabolism up to a redox regulation of bacterial gene expression. [29, 30] In this paper, we focus on coherent ET that is the main component of any type of ET, with or without the system relaxation in the intermediate step. [8] Our results show that incorporation of an iron atom in the form of an iron-sulfur cluster substantially (by several orders of magnitude) increases the protein conductivity at very low bias voltages. They also reveal high similarity in energetics and the efficiency of ET through Fe atom chelated either by four nitrogen atoms of a tetrapyrrole ring or by four sulfur atoms of cysteines in a FeS cluster.

COMPUTATIONAL APPROACHES

The central part of rubredoxin containing FeS cluster was used in our analysis. Optimization of the electronic structures was performed with Gaussian 09 [31] using a Density Functional Theory (DFT) approach with a nonlocal exchange correlation functional comprised of

Becke's three-parameter exchange functional and the Lee−Yang−Parr correlation functional (B3LYP) with 6-31G(d) or LanL2DZ basis set for the iron. [25, 26, 32, 33] The structure for the gold crystal, Au (111), was acquired from QuantumWise's molecular library. [34] The electrodes were assumed to be separated by distance (15.85 Å) that is slightly above the size of the protein fragment inserted between them. In order to best replicate typical electrochemical, STM and conductive AFM experiments, [2, 10, 35-38] one amino acid (Val5) in the studied protein fragment was replaced with cysteine and bound through a thiol group to one electrode. Initially, the electronic structure of isolated rubredoxin fragment was optimized using DFT. Then the protein was attached to the right electrode by placing the S atom of Cys5 at the top of the pyramid connecting it to three Au atoms of the right electrode at distance 2.3 Å and the entire system (the protein and three surface layers of Au from each electrode) were allowed to relax to the minimum energy by using the optimization module in Quantum wise. This module uses molecular dynamics to find a stable position for the molecule and electrodes relative each other. The electrodes themselves are not included in that step, but are implicitly present. [25, 39] This (relaxed) structure was used for calculations the density of states (DOS), energy spectrum, electron transmission spectrum, eigenstates, and transmission paths were performed by including the coupling between the molecular orbitals and the electrodes. For the calculation of ET properties, we utilize a non-equilibrium Green's function (NEGF) approach implemented in Atomistix ToolKit. [34] We use DFT plus NEGF to compute the Green's function self-consistently for the system, and the current is extracted using the Landauer-Büttiker formalism based on these Green's functions, coupling constants and self-energies which are computed according to [39]. This code uses a linear combination of atomic orbitals (LCAO) of the SIESTA type as a basis set. In our calculations, we used a double-ζ basis set with polarization orbitals and the local density approximation (LDA) as parametrized by Perdew−Zunger (PZ) for the exchange correlation functional. For the electronic transport calculations, the system was divided into three regions consisting of the two electrodes and a central scattering region. The electrodes were treated as semi-infinite repetitions of Au (111). The current was calculated for a range of applied bias voltages using the Landauer−Büttiker formula, [15]

$$I(V) = \int T(E,V)[n_f(E-\mu_L) - n_f(E-\mu_R)]dE \quad (1)$$

where n_f is the temperature-dependent Fermi function and μ_L and μ_R are the electrochemical potentials of the left and right electrodes, respectively. The total transmission at each energy level (eigenstate) is given by [39]

$$T(E,V) = Tr[\Gamma_L G \Gamma_R G^+] \quad (2)$$

where the transmission probability is a function of both energy and the applied bias for each converged density of states (DOS) of the entire system. *G* and G^+ are the retarded and advanced Green's functions, which describe the dynamics of the electrons in the central scattering region including the peptide and three layers of gold atoms near each electrode. Γ_L and Γ_R are broadening matrices, which describe the strength of the coupling of each electrode to the conducting scattering region and were calculated as the imaginary parts of the self-energy matrices of the electrodes. The Fermi level for the case of a finite bias voltage is the average of the electrochemical potentials of two electrodes. We use the total transmission spectrum and the density of states to interpret the conductance properties of our systems. The calculations were performed in vacuum at temperatures of 300 and 100 K with periodic boundary conditions in a box measuring 14 × 14 Å in the plane perpendicular to the direction of ET using DoD HPC "Thunder" of SGI type.

The transmission eigenvalues are obtained by diagonalizing the transmission matrix. The number of eigenvalues indicates the number of individual channels going through the molecule; the eigenvalues themselves indicate the strength of each channel. The eigenvalues

are the true transmission probabilities, and thus lie in the interval [0,1]. If several channels are available at a particular energy, at high conductivity their sum, and hence the transmission coefficient at this energy, may however be larger than 1. The effective potential is calculated as the total Kohn-Sham potential that is the sum of the Hartree term (all mean-field electrostatic interactions) and the exchange-correlation potential. [40]

The coupling efficiency (parameters γ_l and γ_r) of the ET peaks in the transmission spectra are estimated from fitting individual peaks to Lorentzian curve

$$T(E) = \Gamma_L\Gamma_R/[(E - \varepsilon_{BAND})^2 + (\Gamma_L + \Gamma_R)^2/4], \qquad (3)$$

where E is the energy relative to the Fermi level, ε_{BAND} is the position of the band, T(E) is a local approximation of the transmission spectra and Γ_L and Γ_R are the electronic coupling strengths to the left and right electrode, respectively. To find the Γ_L and Γ_R parameters, we minimized the integrated square of the deviation $\int(T(E,V) - T_f(E))^2 dE$ around the peaks using Newton's method implemented in the modified package LOQO. [41]

RESULTS AND DISCUSSION

For our calculations we choose rubredoxin, [27, 28, 42] a protein that has a single iron-sulfur cluster of FeS_4 type and the structure of which was estimated crystallographically at 1.6 Å spatial resolution (PDB accession number 6RXN. Though there is a gap in amino acid numbering in original 6RXN, in our work we follow the amino acid numbering defined in this PDB file). For the calculation of ET we consider an FeS cluster and amino acids located within 8 Å from Fe assuming that electron tunneling through distances longer that 9-10 Å is close to zero. [11, 32, 33] It is also consistent with the fact that all known proteins with crystallographically estimated structures have distances for electron hopping between metallic centers within 10-12 Å. [6, 27, 42] According to the crystallographic data, the part of rubredoxin surrounding FeS cluster and used in our calculation has an asymmetric shape with one relatively flat side that we oriented towards the right electrode (Figure 1). For chemical binding to the electrode we use one internal cysteine (Cys38) and one cysteine substituting Val5 (Figure 1). We selected Val5 because it is close to Fe, but outside of Fe-binding signature (CXXC) and it faces the same (right) electrode as the other Cys (Cys38) so we can compare the role of these two cysteines in electron transfer to the same electrode. To check the effect of chemical binding we consider only one of these Cys as bound to the electrode. The second Cys was separated from the electrode by a distance that slightly exceeds 1.65 Å, the length of the S-Au chemical bond (Figure 1).

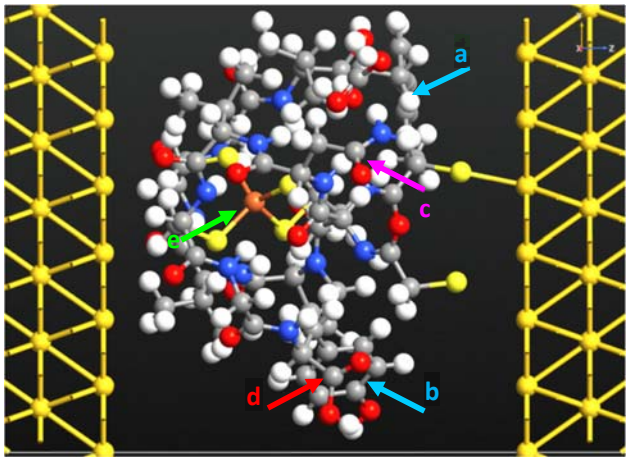

XMQKYCCNVCGYEYDPAEHDNVPFDQLPDDWCCPVCGVSKDQFSPA

Figure 1. Molecular structure of rubredoxin (PDB 6RXN) FeS core consisting of FeS cluster and the nearest located within 8 Å, amino acids. The colored arrows point to positions of aromatic amino acids, Phe (a) and Tyr (b), polar amino acid Asn (c), carboxylic C-end (d) and the FeS cluster (e). Below is rubredoxin core sequence where amino acids located within 8 Å from the FeS cluster are highlighted. For peptide chemical binding to gold (1,1,1) electrode Val5 (of 6RXN) was substituted with Cys.

The apoprotein part of the analyzed rubredoxin core has two aromatic amino acids, Tyr11 and Phe49 and polar amino acids, Asn7. To exclude the effect of local charges from C- and N-terminal ends of the peptide we consider capped C- and N- peptide ends (-COOH and $–NH_2$). The protein was oriented to the electrode in such a way that the ring of one of the aromatic amino acids (Phe49) was oriented parallel to the right electrode surface, while the ring of the other aromatic amino acid (Tyr11) is oriented nearly perpendicular to it (Figure 1). This was achieved by total protein rotation relative to the right electrode

keeping the protein structure intact and relaxed, similar to the native protein. Since the delocalized electronic structure of aromatic amino acids could facilitate their participation in ET, the analysis of these two orientations allows us to estimate the effect of the aromatic ring orientation on the ET efficiency.

to the electrode, c) the role of charged amino acids, and d) the role of the protein backbone.

Energetics of ET: ET transmission energies and efficiencies. The role of protein components.

The electron transmission spectrum (ETS) describes the distribution of molecular electronic energy levels that participate in electron transfer. Besides the protein

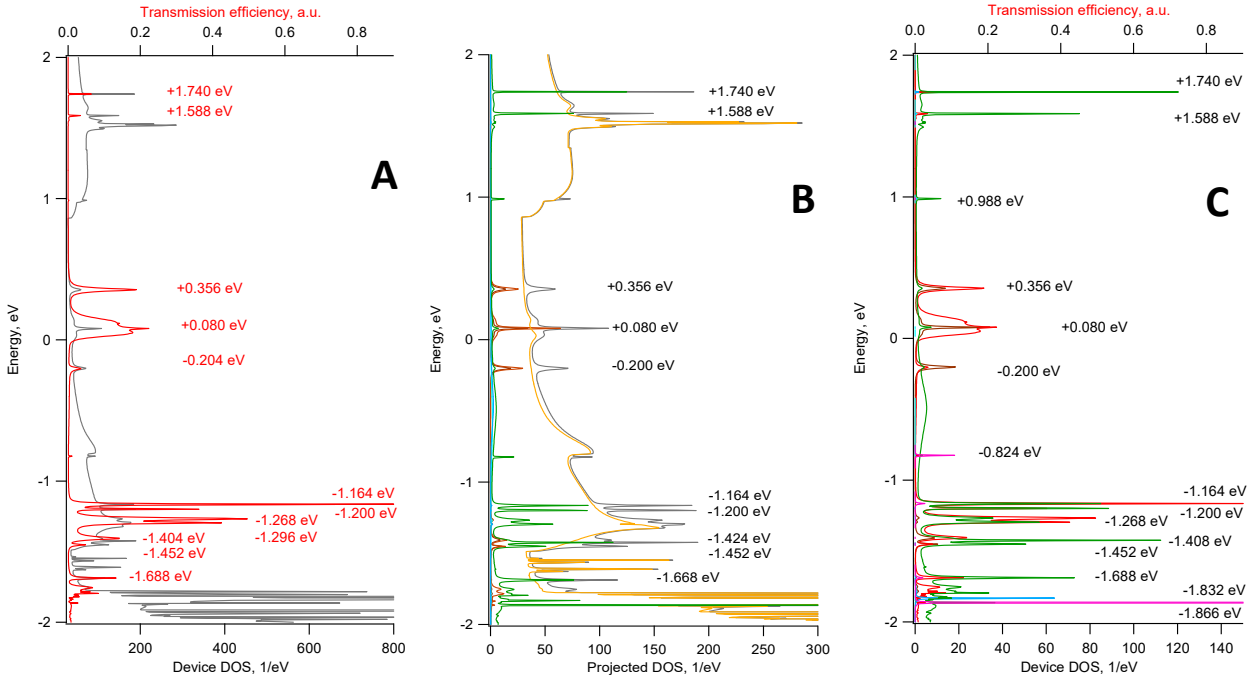

Figure 2 (A) ETS (red, upper scale) and total device DOS (gray, bottom scale) of rubredoxin (PDB 6RXN) with modifications described in the legend to Figure 1 and placed between two gold electrodes as shown in figure 1A. (B) Total DDOS (-) along with DOS projected to Au electrodes (yellow), to apo-protein without FeS cluster (green), FeS cluster (dark red), Fe atom (dark red), and aromatic amino acids Phe (light blue) and Tyr (light blue). The numbers at the peaks indicate energies of the ETS and some DOS peaks. (C) Projected DOS (bottom scale) of FeS cluster, Rd backbone, polar Asn (-) and aromatic amino acids Phe (-) and Tyr (-), along with device ETS (top scale) at zero bias, 300K.

The opposite side of the protein (facing the left electrode) does not have aromatic amino acids. In our configuration, this side is not bound to the electrode, potentially allowing for electron tunneling to/from the electrode through any protein atoms. The FeS cluster is buried inside the protein; it locates rather far from both electrodes (5.66 Å from the left and 10.19 Å from the right electrode) that potentially reduces the efficiency of direct Au-Fe tunneling. Thus, the constructed device allows us to analyze a) the role of the protein shell in electron tunneling to the FeS cluster, b) the role of aromatic amino acids and their ring orientation relative

electronic energies, the ETS depends on the molecule interaction with electrodes and thus depends on the electrode material, Fermi level, thermal distribution of electronic energy levels (that is, the temperature), and the coupling efficiency between the molecule and the electrodes (that is, the height and width of the barrier for tunneling) which all are included in our consideration. At zero bias (no external potential applied between the electrodes) the ETS of the FeS core analyzed in our work has three main transmission bands close to electrode Fermi energy level: at -0.200, +0.08 (with a complex structure), and +0.356 eV. The last two of them have transmission efficiencies about 0.2 (Figure

2A, red curve) indicating that this part of the protein is conductive at very low bias voltages. Farther below the Fermi energy the calculation shows several additional strong conductive bands (with transmission efficiencies between 0.5 and 0.9) located between -1.2 and -1.5 eV indicating the possibility of efficient p^+-type ET through the protein. Also, two narrow small peaks at +1.588 and +1.740 eV (with efficiency 0.05) show some (small) possibility for n^--type conductance at these potentials.

For identification of the protein parts involved in the formation of each transmission band we calculate the device density of states (DDOS) and its projection to various protein substructures (projected density of states, PDOS). The DDOS shows a broad continuum in the areas above +0.8 eV and below 0 eV on top of which the states similar to those identified in the ETS are clearly seen (Figure 2A, gray curve). The PDOS shows that the broad continuum is localized to the gold electrodes (Fig 2B, yellow curve) and thus belongs to the metallic conductor. The narrow peaks on top of the gold DOS are localized to the iron-sulfur cluster (Figure 2B, red curve) and to the apoprotein (Figure 2B, green curve). The intensities of the three main PDOS peaks at +0.356, +0.08 and -0.20 eV are similar to those observed in this area in the total DDOS and in the FeS PDOS, indicating that FeS is the determinant of electronic properties of the protein around the electrode Fermi energy. These peaks have exactly the same positions as the main transmission peaks in the ETS. Similar peaks are missing from the DOS projected to the rest of the protein (apoprotein) or the gold electrodes (Figure 2B, green and yellow curves), showing that the FeS cluster is the only protein part that can contribute to the electron transfer when electrode potentials are very low (near Fermi level).

The PDOS of the aromatic (Phe and Tyr) and polar (Asn) amino acids have peaks at +1.74 and -1.832; +1.588 and +0.988; and -0.828, -1.164, -1.688 and -1.866 eV, respectively (Figure 2C); they correlate well to peaks in the ETS. Most of these peaks overlap in energy position with peaks in the PDOS of the protein backbone, although their intensities (except for peaks of Tyr at -1.688 and Asn at -1.866 eV) are extremely low (about

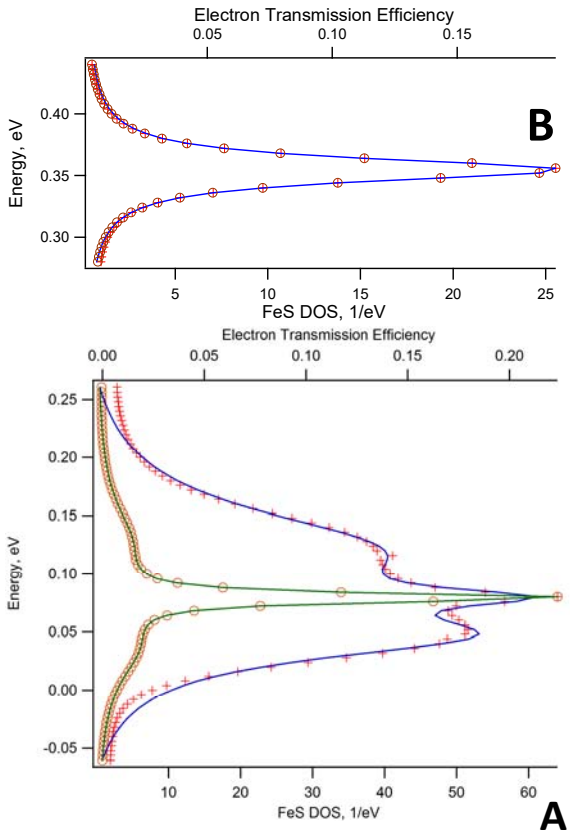

Figure 3. Lorentzian fit (blue and green lines) of FeS DOS (brown circles) and electron transmission bands (red crosses) at (A) 0.356 eV and (B) 0.080 eV.

1/100 of that the peaks of the protein backbone, see PDOS scales in Figure 2B,C and FigureS1) rendering their role in ET insignificant. Nevertheless, to test the possibility of a contribution of these amino acids to the protein conductance, we calculate the multichannel contribution in each of the main ETS bands (Table S1). This calculation shows that for each transmission peak, the main component is about 100x stronger than the second one in intensity, confirming that within 1% accuracy, the apoprotein backbone along with the FeS are the main contributors to the protein conductance for all strong ETS peaks. On the other hand, the peaks at -1.688 and at -1.866 eV in PDOS are much stronger for Tyr and Asn than for the protein backbone, suggesting a possible participation of these amino acids in protein conductivity at these energies. It is important to note that the calculated transmission peaks look relatively high for a molecule without conjugated bonds. But besides MO delocalization several other factors

contribute to the efficiency of ET, the overlap of orbitals which can be favorable or unfavorable for very specific energy intervals (even individual sharp levels), and tunneling through space which is more or less energy-independent and just exponentially attenuating are among them. This will be addressed in the following sections.

Protein-electrode coupling

Protein-electrode coupling is the main parameter controlling the efficiency of ET between the protein and the electrodes. [17] A way to estimate the strength of this parameter is from the shape of ET bands. [25, 32, 33] We found that the bands in rubredoxin ETS can be well described by a Lorentzian shape (see equation 3 and Figure 3). For instance, the band at +0.355 eV has a coupling to the left and right electrode equal to 112 x 10^{-5} and 2119 x 10^{-5} eV (Figure 3, Table 1) which corresponds to ET rates between the protein and electrode ($k = \Gamma/\hbar$) of 1.704 x 10^{-12} and 32.184 x 10^{-12} sec^{-1}. Similar results can be obtained for the other transmission bands. All of them show very efficient coupling and, accordingly, very high rate of ET (Table 1).

One specific interesting feature of the rubredoxin FeS transmission spectrum is a substantial increase of the transmission in the area surrounding the band at 0.080 eV (Figure 3). A similar effect, though much less pronounced, is seen at these energies in the FeS PDOS (Figure3). This broadening should lead to substantial increase in coupling of the FeS MO to the electrodes and thus the efficiency of ET. [25] Indeed, our calculation predicts a coupling constants of the broad band at 0.121 eV which is two times stronger, and at 0.046 eV which is about six times stronger, than that of the narrow bands at +0.355 or +0.080 eV (Table 1). One of the possible explanations of the transmission band broadening is the presence of several parallel paths going through the left and right parts of the apoprotein shell connecting the FeS cluster to the electrodes. Indeed, the presence of the same three characteristic Fe transmission bands at similar positions (+0.37, +0.05, -0.38 eV), but without the broad band in the ETS of heme (an iron chelated by a tetrapyrrole) that do not have protein shell [26] confirms this conclusion and show that the shortening ET tunneling barrier is due to MO delocalization through both FeS and amino acids.

Table 1. Lorentzian fit parameters and calculated couplings (ET rates) between the protein and left and right electrodes for various transmission bands (indicated by energy, E) at bias = 0.

	E, eV	Γ_1 x10^{-5}, eV	Γ_2 x10^{-5}, eV	K_1 x10^{12}, s^{-1}	K_2 x10^{12}, s^{-1}
ETS	**+1.58620**	**9.37**	**139.2**	**0.142**	**2.112**
ETS	**+0.35456**	**112.2**	**2119.1**	**1.704**	**32.184**
ETS	**+0.12078**	**193.5**	**4523.5**	**2.939**	**68.700**
FeS DOS	+0.12753	877.4	14794.5		
ETS	**+0.07959**	**51.8**	**1844.7**	**0.787**	**28.016**
FeS DOS	+0.07916	30.2	7467.0		
ETS	**+0.04638**	**299.0**	**8320.3**	**4.541**	**126.363**
FeS DOS	+0.03695	1091.8	14925.5		
ETS	**-1.6878**	**29.6**	**835.3**	**0.449**	**12.675**

The general feature revealed by the results described above is an extremely high efficiency of FeS coupling to the electrode, especially when taking into account the considerable distances between the Fe atom in the FeS cluster and the left and the right electrodes (5.651 and 10.191 Å, respectively). A possible explanation of this high efficiency might be the coupling between FeS and the electrode through the protein backbone that leads to a higher efficiency due to decrease in the height of the tunneling barrier compared to vacuum.

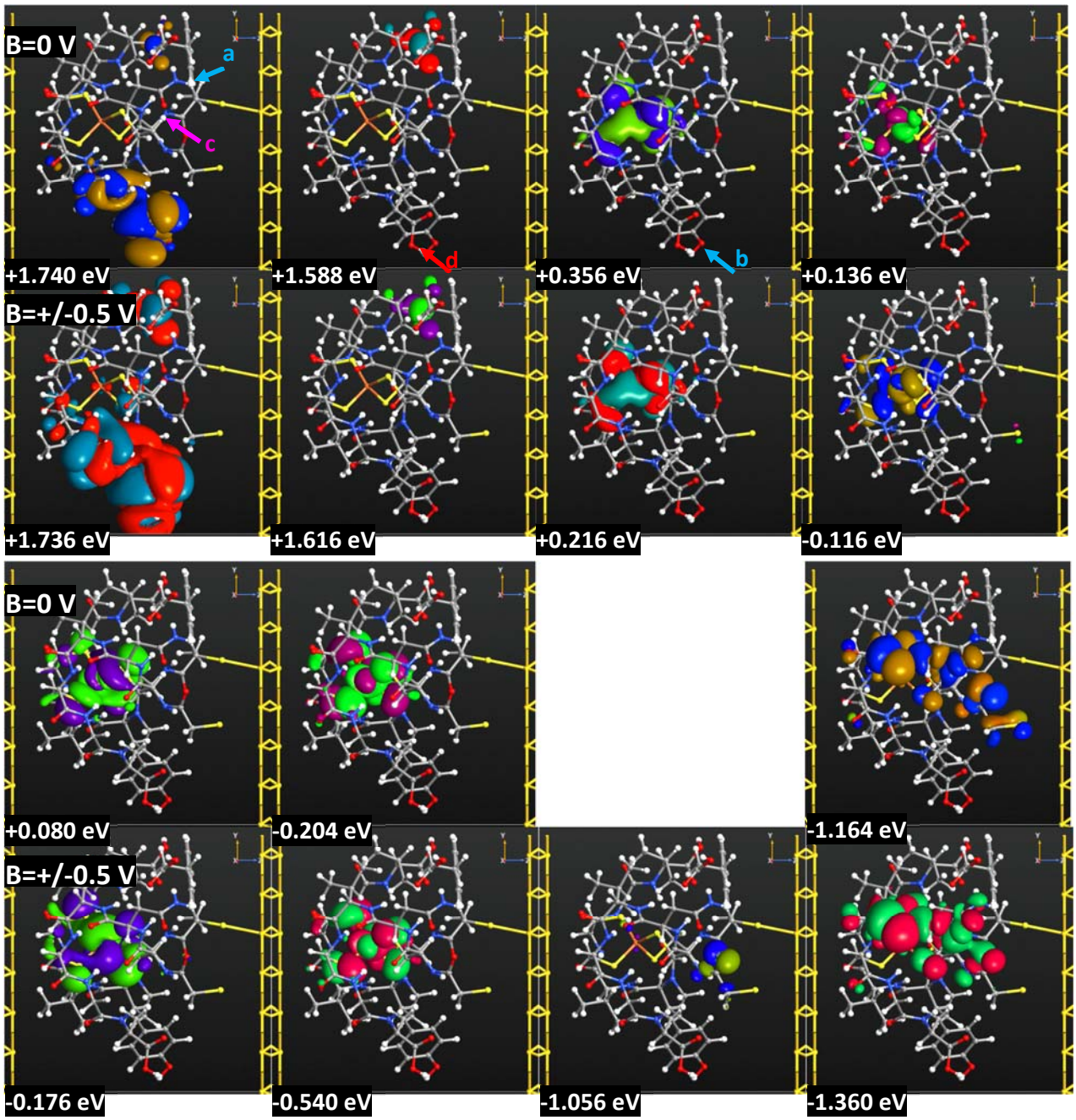

Figure 4. Spatial distribution of molecular transmission eigenstates (at isovalue = 1.0) forming individual transmission peaks at electrode potentials B = 0 V (top rows) and corresponding peaks at electrode potentials B = +/-0.5 V (bottom rows); the first sign corresponds to the polarity of left electrode, temperature 300K. The arrows in the three top left panels point to the aromatic amino acids Phe (a) and Tyr (b), polar amino acid Asn (c), and carboxylic C-end (d). The numbers inside the panels show the energies of the transmission peaks.

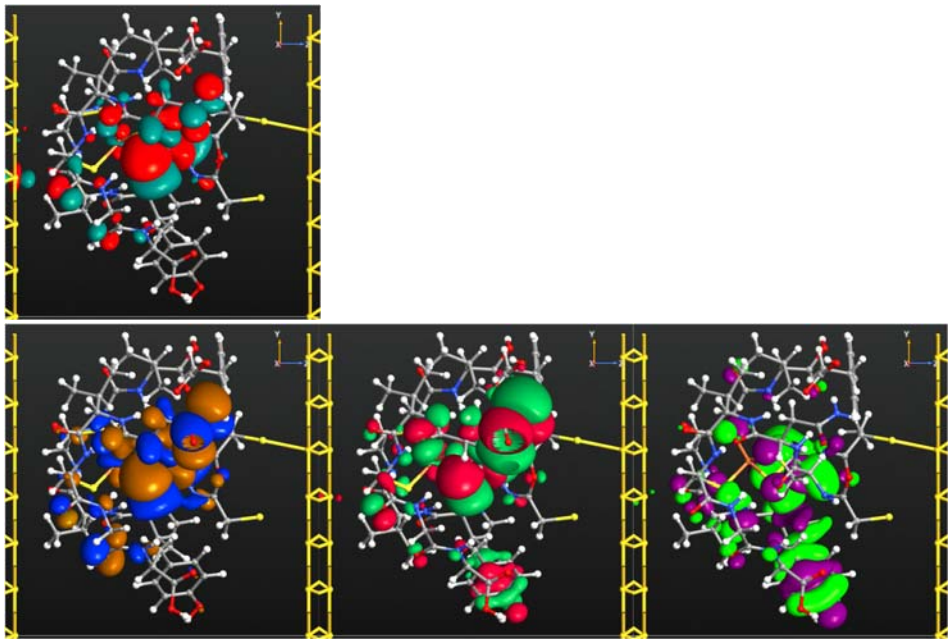

Figure 4 (continued).

Spatial organization of ET: MO delocalization and ET paths

B=0 V

In many molecules, electronic orbital spreading over the entire molecule (delocalization) can substantially improve the ET efficiency by reducing the width of the barrier electron has to tunnel between the molecule and the electrodes. [7, 25] To estimate this effect and to confirm which atoms are involved in ET through the FeS cluster in the protein core, we calculate the transmission e-1.688 eV for different transmission energies (Figure 4B=+/-0.5 V demonstrate a strong contribution from iron atomic orbitals (AOs) in all transmission bands located around the Fermi level (+0.216, +0.136, +0.080 and -0.204 eV). In addition, Fe AOs contribute to strong conductive MOs below the Fermi level (at -1.164 and -1.688 eV). Moreover, better delocalization of the last two bands in the Z-direction (perpendicular to the e-1.716 eV surfaces) correla-1.796 eV a substantial increase in the transmission efficiency of these bands seen in the ETS (Figure 5). On the other hand, weakly conductive bands (particularly, at +1.740 and +1.588 eV) do not contain iron AOs, even if some of them (particularly, the band at +1.740 eV) have considerable delocalization through the peptide. Consistent with the PDOS (Fig 2C), neither of the strong conductive bands delocalizes through Tyr or Phy, (Figure 2A), but MOs of polar Asn seems to be active in the ET at -1.164 and -1.688 eV (Figure 4, top rows).

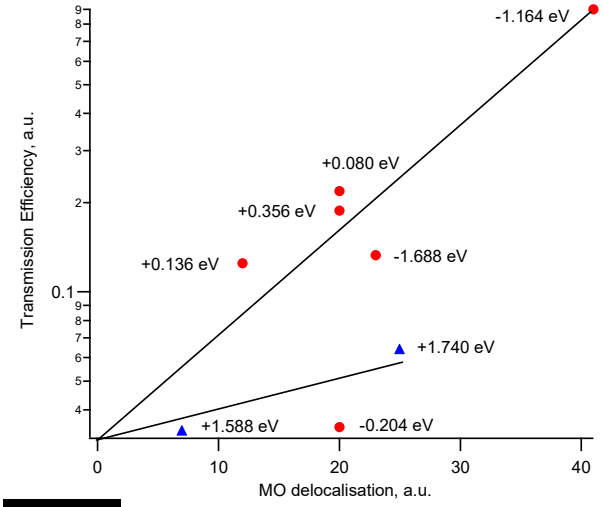

-1.848 eV

Figure 5 Correlation between MO (transmission eigenstate) delocalisation in Z-direction (perpendicular to the electrodes) and the efficiency of ET for MOs including (●) and not including (▲) the FeS cluster. The numbers near the points indicate ET energies. Electrode potentials = 0, temperature = 300K.

All these results indicate that the high efficiency of ETS bands located around the Fermi level is due to the presence of iron AOs. They confirm that these transmission bands belong to the FeS cluster, as the

PDOS shows. Moreover, they indicate that the FeS coupling to the electrode is highly efficient and can occur at rather big distances between the Fe atom and the electrodes. On the other hand, the MOs contributing to the ETS far from the Fermi level and belonging to the protein backbones (disregarding FeS) are relatively inefficient and need to be well delocalized to provide any improvement to the electron transmission. At the same time, the very low transmission efficiency of the band at -0.204 eV from the expected from correlation (Figure 5) is rather significant, indicating that other parameters have a considerable contribution to the ET efficiency of this band. One of these parameters (as the coupling efficiency shows) might be the multiplicity of ET paths. Another factor might be the height of the electron tunneling barrier, specifically whether the electron has to travel through the rest of the molecule or through vacuum. A third parameter decreasing the ET efficiency might be loops in the electron transmission pathways (ETP). [25, 43-45]

To check these possibilities, we calculated ETPs [43] for each transmission band (Figure 6). These calculations confirm that all the strongest transmission paths go through Fe. In addition, they reveal multiple transition paths between the molecule and the electrodes for ET bands at +0.132, +0.080 eV compared to the -0.204 eV band and for the band at -1.164 eV that explains the substantial increase in their efficiency. The ETPs also show that neither Tyr nor Phe is really involved in the electron transfer. In addition, they demonstrate a possibility of ET through the peptide carboxylic group (see ETPs at +1.740 and +1.588 eV), though the efficiency of ET through this group is low partially due to ET reversibility (cf. the arrow thicknesses showing the ET intensity and color showing the ET direction for ETPs at +1.740 and +1.588 eV). Similar reversibility (looping due to the presence of oxygen) reduces the ET efficiency of the -1.688 eV transmission band. These results allow us to conclude that despite high electron concentration and well delocalized MOs at the carboxylic group, the total efficiency of ET through it is still relatively low due to the formation of the ET loop preventing a straight electron movement. [25] Analysis of the ETPs also confirms that the ET through the peptide backbone is much more efficient than tunneling through space. [36, 46]

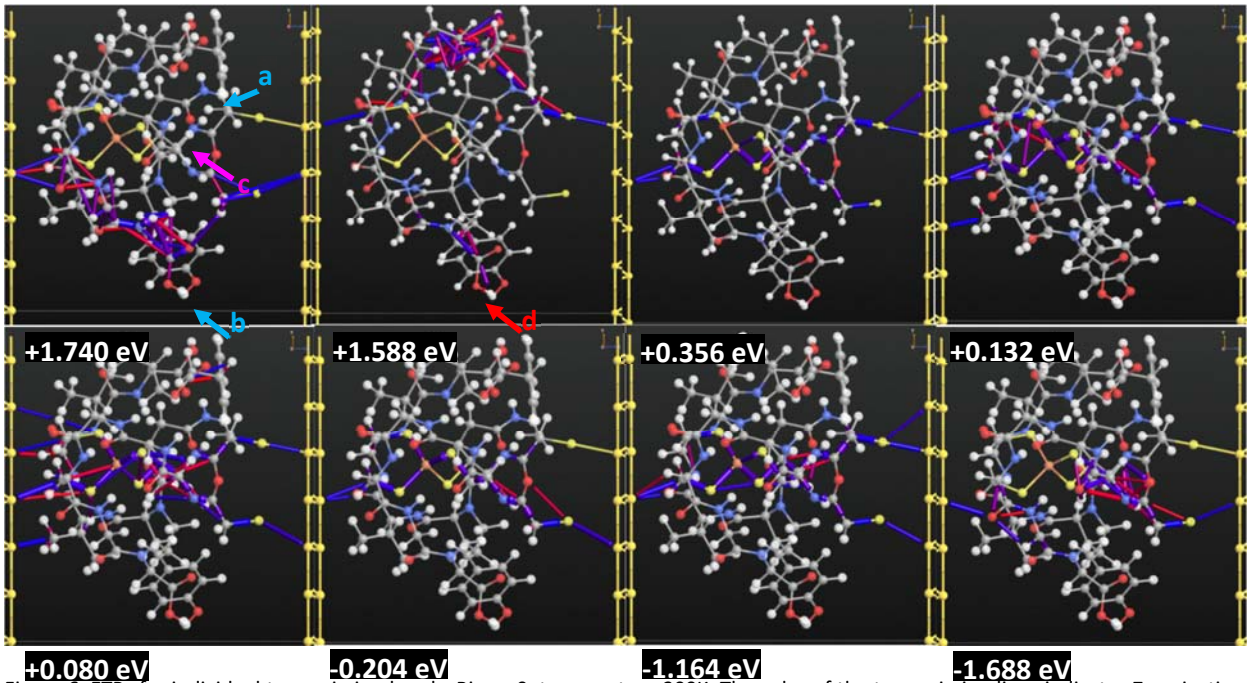

Figure 6. ETPs for individual transmission bands. Bias = 0, temperature 300K. The color of the transmission lines indicates Z-projection of the transmission direction (blue to the right, magenta to the left); the thickness of the line indicates transmission efficiency. The arrows in the two top left panels point to the aromatic amino acids Phe (a) and Tyr (b), polar amino acid Asn (c), and carboxylic C-end (d). The numbers inside the panels show the energies of the transmission peaks.

Effects of local potentials and temperature

Applying a bias voltage to the electrodes substantially affects the rubredoxin ETS. The transmission bands in its central area (±0.5 eV around Fermi), where, as we have shown, ET goes through the FeS cluster, shift to a lower energy when we apply a +0.5 V bias (the sign indicates potential on the left electrode) which results in a substantial increase in their ET efficiency (Figure 7). This bias also narrows the broad transmission bands. A bias with opposite electrode polarity instead shifts the bands up and leads to a reduced transmission efficiency of each band.

We interpret these effects as the result of the overlap between the gradient of the electrostatic field generated by the charged electrode and the internal potential distribution reached at zero bias, particularly with the local fields generated by N and O atoms of peptide bonds oriented perpendicular to the electrodes. If this is the case, a positive bias (+0.5 V) should much less affect the protein transmission bands located outside this area. Indeed, compared to the ETS bands belonging to FeS cluster, the position of the bands belonging to the protein shell (backbone) that are located at about +1.6 through +1.8 and -1.5 through -1.8 eV are much less sensitive to the applied bias voltage (Figure 7). The only effect that is observed for these bands is a change in their transmission efficiency, especially at positive bias (+ on the left electrode and – on the right) which might be due to a modulation of their eigenstate spatial distribution. To test this possibility and to identify the origin of the bands in ETS under applied electrode potentials, we calculate transmission eigenstates of individual transmission bands and compare them to the eigenstates observed at zero bias (Figure 4, bottom rows). As expected, ET through the bands at +1.6 through +1.8 and -1.5 through -1.8 eV goes around FeS cluster. As expected, we also observe a good similarity of the eigenstate shapes and delocalization of the FeS bands at different electrode potentials, confirming that the change in the conductivity is due to the overlap of the external electric field with their MO energy. On the other hand, this calculation reveals a substantial increase in the electron density on Tyr eigenstates located at -1.796 and -1.848 eV (Figure 4).

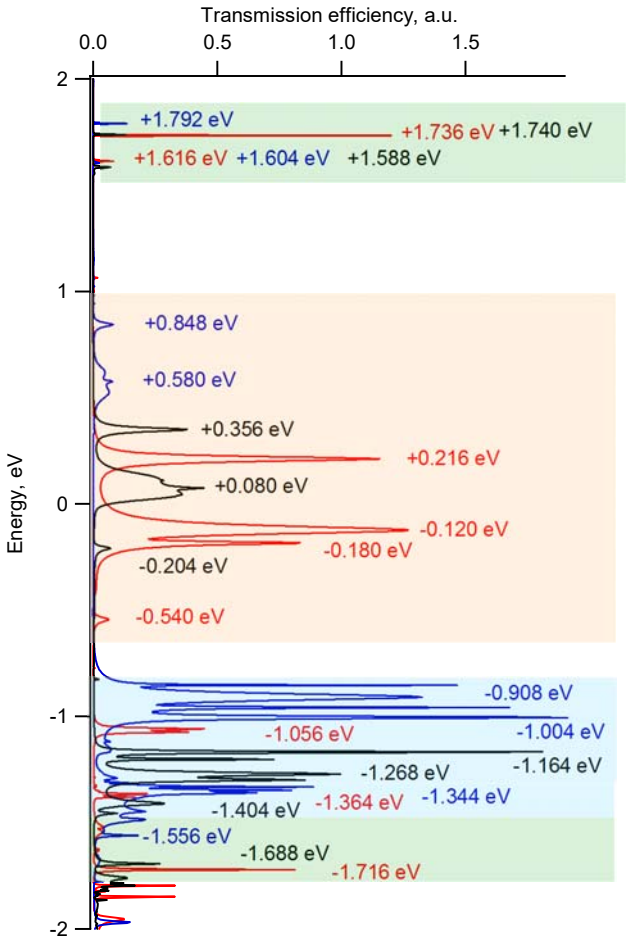

Figure 7. ETS at different electrode potentials (bias voltages) (-/+0.5 V, blue, 0/0 V, black, +/-0.5 V, red; the first sign in the notation is for the polarity of the left electrode).

Applying bias voltages to the electrodes allows for calculation of an electric current going through the protein (Table 2). At +/- 0.5 V and -/+ 0.5 V the calculations give values 5878 nA and 127 nA. The first of these values corresponds to about 10% of the theoretical maximum for a single molecular conductor (77 nS) [17] confirming the experimentally observed high conductivity of FeS proteins [11] and predicted enhancement of peptide conductivity in the presence of Ni and Cu ions. [47, 48] It also shows an important role of iron in protein conductivity since these values are about 6 to 9 orders of magnitude higher than estimated for pilA protein fragments without Fe. [25] The other interesting result coming from this calculation that confirms the previous estimations [7, 25] is the difference of the current at the two polarities, which shows that

the protein transmits current in only one direction (efficiency 50:1). This ability of the protein core to generate a unidirectional current explains why iron-based proteins can operate so wisely and efficiently in highly complex multidimensional and multicomponent biological systems.

Table 2. Calculated current through rubredoxin core at bias voltages -0.5 V and +0.5 V and temperatures 300 and 100 K. In the table head the first sign corresponds to the polarity of the left electrode. The plus sign of the current indicates direction of ET to the left electrode.

-/+ 0.5 V, at 300K	+/- 0.5 V, at 300K	+/- 0.5 V, at 100K
-0.127 μA	5.878 μA	5.894 μA

Temperature-induced change of electrode occupancies could lead to a considerable alteration of the molecular coupling to the electrodes. To test this possibility we calculate the effect of temperature (100 K vs. 300 K) on various ET bands at bias potential +/- 0.5 V. The results show no effect of temperature (neither on the energy, nor on ET efficiency) on most of the transmission bands, including those belonging to the FeS cluster and the protein backbones (Figure S1C). At the same time, the efficiency of electron transfer considerably reduces for the bands at +1.736 eV and increases for the bands at -1.716 and -1.852 eV confirming the prediction that electron tunneling through aromatic amino acid might be temperature-dependent.

Conclusions

The obtained results show that an iron atom incorporated into the protein structure as an iron-sulfur cluster opens a transmission path at the Fermi energy level of the electrodes. This allows the protein to become an extremely efficient conductor at very low bias voltages (<$\pm$0.35 V). The conductivity of the protein containing the FeS cluster is compatible with the theoretical limit of molecular conductance. Four major factors contribute to the high conductivity of FeS-containing proteins: 1) the close location of the Fe transmission bands to the electrode Fermi level; 2) a considerable delocalization of its MO through FeS and the surrounding amino acids leading to shortening width of the barrier electron has to tunnel; 3) the presence of the protein backbone which reduces the tunneling barrier height; and 4) the presence of several parallel ET paths which increases the efficiency of the Fe coupling to the electrode. Though the FeS cluster appears to be the only ET mediator at low bias, direct ET through the surrounding amino acids bypassing FeS is possible at biases $\pm$1.5 to $\pm$2 V. Neither aromatic Tyr, nor Phe participate in ET through the studied FeS protein core. Some MO of polar Asn might participate in ET at high bias voltages. Though the exact values of ET rate might change if intermediate (hopping) steps are taken into account, [10] the general principle described here will hold for any type of ET. The conductivity of the protein core substantially depends on the polarity of the applied electric field allowing for unidirectional ET and operation of the protein as a molecular rectifier. [7] Our results show that this effect is mainly due to a substantial shift of the FeS electronic energy levels by the electrostatic potentials of the surrounding electrodes. Thus the described protein core represents a highly conductive molecular unit. This unit is enough for the construction of efficient protein-based molecular wires and other quantum electronic devices; and it can be used for wise *de novo* construction of new proteins for molecular electronics and cellular energy converting devices.

Conflicts of interest

We have no conflicts to declare.

Acknowledgements

This work was supported by NRL, ONR, and DoD HPC programs.

References

1. T. Brixner, J. Stenger, H. M. Vaswani, M. Cho, R. E. Blankenship and G. R. Fleming, *Nature*, 2005, **434**, 625-628.
2. Y. A. Gorby, S. Yanina, J. S. McLean, K. M. Rosso, D. Moyles, A. Dohnalkova, T. J. Beveridge, I. S. Chang, B. H. Kim, K. S. Kim, D. E. Culley, S. B. Reed, M. F. Romine, D. A. Saffarini, E. A. Hill, L. Shi, D. A. Elias, D. W. Kennedy, G. Pinchuk, K. Watanabe, S. Ishii, B. Logan, K. H. Nealson and J. K. Fredrickson, *Proc. Natl. Acad. Sci. U. S. A.,* 2006, **103**, 11358-11363.

3. D. R. Lovley, in *Annu. Revi. Microbiol., Vol 66*, eds. S. Gottesman, C. S. Harwood and O. Schneewind, 2012, vol. 66, pp. 391-409.
4. M. D. Yates, B. J. Eddie, N. J. Kotloski, N. Lebedev, A. P. Malanoski, B. C. Lin, S. M. Strycharz-Glaven and L. M. Tender, *Energy Environ. Sci.*, 2016, **9**, 3544-3558.
5. R. A. Marcus and N. Sutin, *Bioch. Biophys. Acta*, 1985, **811**, 265-322.
6. C. C. Moser, J. M. Keske, K. Warncke, R. S. Farid and P. L. Dutton, *Nature*, 1992, **355**, 796-802.
7. G. T. Feliciano, A. J. R. da Silva, G. Reguera and E. Artacho, *J. Phys. Chem. A*, 2012, **116**, 8023-8030.
8. D. N. Beratan, C. Liu, A. Migliore, N. F. Polizzi, S. S. Skourtis, P. Zhang and Y. Zhang, *Accounts Chem. Res.*, 2014, **48**, 474-481.
9. Y. Zhang, C. Liu, A. Balaeff, S. S. Skourtis and D. N. Beratan, *Proc. Natl. Acad. Sci. U. S. A.*, 2014, **111**, 10049-10054.
10. S. Pirbadian, S. E. Barchinger, K. M. Leung, H. S. Byun, Y. Jangir, R. A. Bouhenni, S. B. Reed, M. F. Romine, D. A. Saffarini, L. Shi, Y. A. Gorby, J. H. Golbeck and M. Y. El-Naggar, *Proc. Natl. Acad. Sci. U. S. A.*, 2014, **111**, 12883-12888.
11. A. Petrenko and M. Stein, *J. Phys. Chem. B*, 2015, **119**, 13870-13882.
12. A. Rana, S. Dey, A. Agrawal and A. Dey, *J. Biol. Inorg. Chem.*, 2015, **20**, 1147-1162.
13. M. Breuer, K. M. Rosso, J. Blumberger and J. N. Butt, *J. Royal Soc. Interface*, 2015, **12**, Article number 20141117.
14. H. C. Yan, C.; Zhugayevych, A.; Tretiak, S.; Dahlquist, F.W.; Bazan, G.C., *Adv. Mater.*, 2015, **27**, 1908-1912.
15. M. Buttiker, Y. Imry, R. Landauer and S. Pinhas, *Phys. Rev. B*, 1985, **31**, 6207-6215.
16. A. Nitzan and M. A. Ratner, *Science*, 2003, **300**, 1384-1389.
17. S. Datta, *Quantum Transport: Atom to Transistor* Campbridge University Press, 2009.
18. R. Venkatramani, E. Wierzbinski, D. H. Waldeck and D. N. Beratan, *Faraday discussions*, 2014, **174**, 57-78.
19. S. Gosavi and R. A. Marcus, *J. Phys. Chem. B*, 2000, **104**, 2067-2072.
20. R. M. Snider, S. M. Strycharz-Glaven, S. D. Tsoi, J. S. Erickson and L. M. Tender, *Proc. Natl. Acad. Sci. U. S. A.*, 2012, **109**, 15467-15472.
21. S. S. Skourtis, D. N. Beratan, R. Naaman, A. Nitzan and D. H. Waldeck, *Phys. Rev. Lett.*, 2008, **101**, Article number 238103.
22. N. F. Polizzi, S. S. Skourtis and D. N. Beratan, *Faraday Discussions*, 2012, **155**, 43-62.
23. P. S. Bonanni, D. Massazza and J. P. Busalmen, *Phys. Chem. Chem. Phys.*, 2013, **15**, 10300-10306.
24. L. M. Xiang, J. L. Palma, C. Bruot, V. Mujica, M. A. Ratner and N. J. Tao, *Nature Chem.*, 2015, **7**, 221-226.
25. N. Lebedev, S. Mahmud, I. Griva, A. Blom and L. M. Tender, *J. Polymer Sci. B-Polymer Phys.*, 2015, **53**, 1706-1717.
26. N. Lebedev, Griva, I., Blom, A., *J. Phys. Chem. C*, 2013, **117**, 6933-6939.
27. P. Zanello, *Coord. Chem. Rev.*, 2014, **280**, 54-83.
28. L. Altamura, C. Horvath, S. Rengaraj, A. Rongier, K. Elouarzaki, C. Gondran, A. L. B. Macon, C. Vendrely, V. Bouchiat, M. Fontecave, D. Mariolle, P. Rannou, A. L. Goff, N. Duraffourg, M. Holzinger and V. Forge, *Nature Chem.*, 2017, **10**, 157-163.
29. E. L. Carter and S. W. Ragsdale, *J. Inorg. Biochem.*, 2014, **133**, 92-103.
30. M. T. Stiebritz, *Nucleic Acids Res.*, 2014, **42**, 5426-5435.
31. M. J. Frisch, G. W. Trucks, H. B. Schlegel, G. E. Scuseria, M. A. Robb, J. R. Cheeseman, G. Scalmani, V. Barone, B. Mennucci, G. A. Petersson, H. Nakatsuji, M. Caricato, X. Li, H. P. Hratchian, A. F. Izmaylov, J. Bloino, G. Zheng, J. L. Sonnenberg, M. Hada, M. Ehara, K. Toyota, R. Fukuda, J. Hasegawa, M. Ishida, T. Nakajima, Y. Honda, O. Kitao, H. Nakai, T. Vreven, J. A. Montgomery, Jr., J. E. Peralta, F. Ogliaro, M. Bearpark, J. J. Heyd, E. Brothers, K. N. Kudin, V. N. Staroverov, R. Kobayashi, J. Normand, K. Raghavachari, A. Rendell, J. C. Burant, S. S. Iyengar, J. Tomasi, M. Cossi, N. Rega, J. M. Millam, M. Klene, J. E. Knox, J. B. Cross, V. Bakken, C. Adamo, J. Jaramillo, R. Gomperts, R. E. Stratmann, O. Yazyev, A. J. Austin, R. Cammi, C. Pomelli, J. W. Ochterski, R. L. Martin, K. Morokuma, V. G. Zakrzewski, G. A. Voth, P. Salvador, J. J. Dannenberg, S. Dapprich, A. D. Daniels, Ö. Farkas, J. B. Foresman, J. V. Ortiz, J. Cioslowski, and D. J. Fox, Gaussian 09, Gaussian, Inc., Wallingford CT, 2009.

32. N. Lebedev, I. Griva, G. S. Kedziora, A. Blom and J. M. Schnur, *J. Phys. Chem. C*, 2010, **114**, 22710-22717.
33. N. Lebedev, I. Griva, S. A. Trammell, G. S. Kedziora, L. M. Tender and J. Schnur, *J. Phys. Chem. C*, 2010, **114**, 12341-12345.
34. Atomistix ToolKit version 2008.10, QuantumWise A/S 2008.
35. N. Lebedev, S. A. Trammell, A. Spano, E. Lukashev, I. Griva and J. Schnur, *J. Amer. Chem. Soc.*, 2006, **128**, 12044-12045.
36. M. Y. El-Naggar, G. Wanger, K. M. Leung, T. D. Yuzvinsky, G. Southam, J. Yang, W. M. Lau, K. H. Nealson and Y. A. Gorby, *Proc. Natl. Acad. Sci. U. S. A.*, 2010, **107**, 18127-18131.
37. J. P. Veazey, G. Reguera and S. H. Tessmer, *Phys. Rev. E*, 2011, **84,** Article number 060901.
38. N. S. Malvankar, M. T. Tuominen and D. R. Lovley, *Energy Environ. Sci.*, 2012, **5**, 8651-8659.
39. M. Brandbyge, J. L. Mozos, P. Ordejon, J. Taylor and K. Stokbro, *Phys. Rev. B*, 2002, **65,** Article number 165401.
40. W. Kohn and L. J. Sham, *Phys. Rev.*, 1965, **140**, 1133-1138.
41. I. Griva, *Computational Optimization and Applications*, 2004, **29**, 173-195.
42. J. Liu, S. Chakraborty, P. Hosseinzadeh, Y. Yu, S. L. Tian, I. Petrik, A. Bhagi and Y. Lu, *Chem. Rev.*, 2014, **114**, 4366-4469.
43. S. G. Chen, Y. Zhang, S. Koo, H. Tian, C. Y. Yam, G. H. Chen and M. A. Ratner, *J. Phys. Chem. Lett.*, 2014, **5**, 2748-2752.
44. G. C. Solomon, C. Herrmann, T. Hansen, V. Mujica and M. A. Ratner, *Nature Chem.*, 2010, **2**, 223-228.
45. H. Schlicke and C. Herrmann, *ChemPhysChem*, 2014, **15**, 4011-4018.
46. A. Migliore, N. F. Polizzi, M. J. Therien and D. N. Beratan, *Chem. Rev.*, 2014, **114**, 3381-3465.
47. X. Y. Xiao, B. Q. Xu and N. J. Tao, *Angew. Chem., Int. Ed.*, 2004, **43**, 6148-6152.
48. T. M. Perrine and B. D. Dunietz, *Nanotechnology*, 2007, **18,** Article Number 424003.

Nikolai Lebedev, Igor Griva, Anders Blom, and Leonard M. Tender " Effect of Iron Doping on Protein Molecular Conductance" TOC Picture:

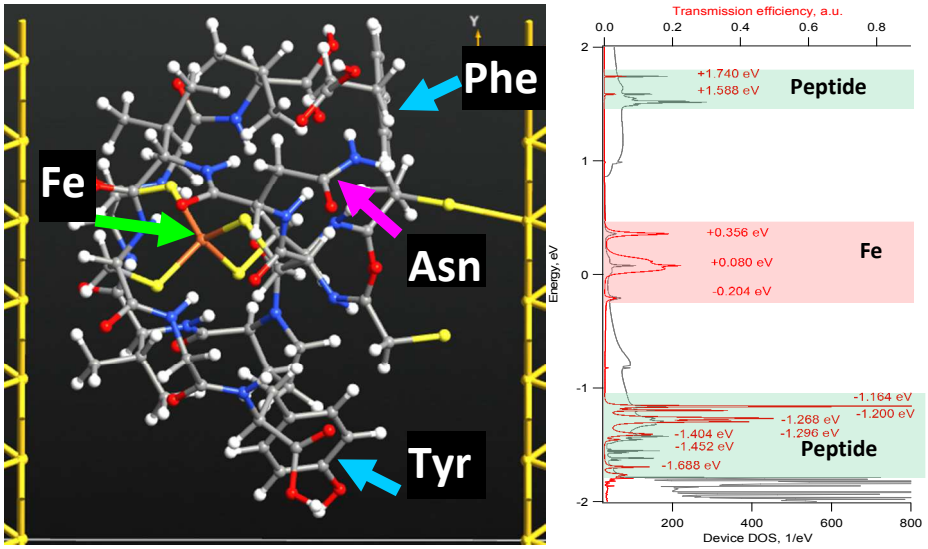

This study analyzes the role of Fe in electron transfer through non-heme iron-containing proteins.